THE JOURNAL OF PHYSICAL CHEMISTRY C

Article

Cite This: J. Phys. Chem. C 2019, 123, 18551−18559

pubs.acs.org/JPCC

Neutron Diffraction Study on the Magnetic Structure of the Promised Multiferroic Hybrid Perovskite $[C(ND_2)_3]Cu(DCOO)_3$ and Its Centrosymmetric Analogues

M. Viswanathan,*[,†] Shwetha G. Bhat,[‡] A. K. Bera,[¶] and Juan Rodríguez-Carvajal[§]

[†]School of Physics and Astronomy, Queen Mary University of London, London E1 4NS, United Kingdom

[‡]Department of Physics, Indian Institute of Science, Bangalore 560012, India

[¶]Solid State Physics Division, Bhabha Atomic Research Centre, Mumbai 400085, India

[§]Diffraction Group, Institut Laue Langevin, 71 Avenue des Martyrs, 38042 Grenoble, France

Supporting Information

ABSTRACT: This report presents with one of the rare experimental studies on the magnetic structure of hybrid framework materials, $[C(ND_2)_3]Me^{2+}(DCOO)_3$ (Me = Cu, Mn, and Co), by using neutron powder diffraction. Copper guanidinium formate (CuGF) having a polar structure is a promised multiferroic member of the hybrid perovskite metal guanidinium formates and its Mn/Co analogues possessing a centrosymmetric structure. Previous investigations based on *ab initio* calculations have suggested that CuGF is a multiferroic whose magnetic space groups are assignable either to $Pn'a'2_1$ or $Pna'2_1'$. Our neutron experiments concurrently reject the $Pna'2_1'$ possibility and suggest the magnetic structure of CuGF as either $Pna2_1$ or $Pn'a'2_1$, with both exhibiting "Type-A" magnetic ordering, free from ferromagnetic ordering along the polar-axis, with spins lying in the *ab* plane. In contrast to CuGF, its centrosymmetric analogues Mn/CoGF are found to display "Type-G" magnetic ordering, with their spins aligned along the *b* and *c* axis, respectively. The in-depth evaluation of magnetic structure of the metal guanidinium formate frameworks could be helpful in the understanding and designing of the magnetic functionalities of multiferroic hybrid perovskites and could provide an encouraging platform for the improvement of *ab initio* studies.

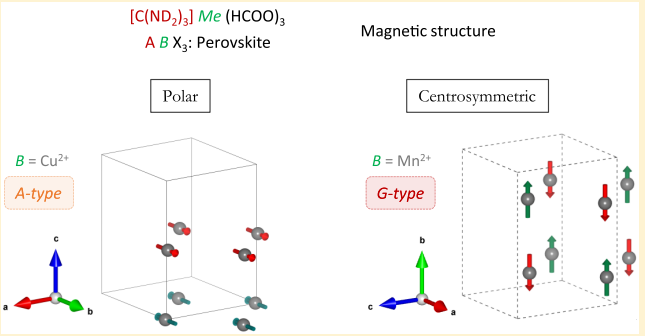

INTRODUCTION

In recent years, materials known as multiferroics that simultaneously exhibit both magnetic and electrical ordering have advanced with technological ambitions.[1] Most of them existing in an inorganic form suffers particularly from the lack of magnetic tunability. Nevertheless, metal−organic frameworks (MOFs), a hybrid class of materials consisting of both organic and inorganic components, are considered as promising alternatives with desired properties. Such an appreciable resultant develops from the organic−inorganic duality,[2] which harvests a vast potential to create new materials by modifying the inorganic/organic component ratio.[3] Therefore, in general, MOFs can be tailored to exhibit desirable properties, such as tuning of the magnetic coupling.[4]

While the magnetic structures on plenty of perovskite oxides such as $AMnO_3$ (A = La, Sr, Tb, Y)[5−8] are reported since the 1950s, some of the double perovskites such as $A_2BB'O_6$ (A = Sr, Ca; B/B′ = Fe, Mo, Mn, W)[9−11] have caught attention in the past decade. Down this route, the magnetic structure of complex multiferroic oxides have also begun to unfold.[12−16] While the scientific community continues to emphasize on the determination of magnetic structures in oxides,[5−16] the scenario for hybrid materials is quite different, a setting that has resulted in the magnetic structure determination of hybrid materials, be in its infancy, therefore lacking a substantial input for designing multiferroic/magnetic functionalities.

Formate ($HCOO^-$) is the simplest carboxylic ligand and can acquire different bridging modes, resulting in the formation of different framework structures and, hence, properties. Since the discovery of multiferroic characteristics in $[(CH_3)_2NH_2]Me(HCOO)_3$ [Me = Mn, Co, Fe, Ni],[17] perovskite-type formate-based MOFs are considered as potential candidates for ferroic applications. Guanidinium $[C(NH_2)_3]^+$ forms three pairs of strong hydrogen bonds linked to various oxyanions, acting as connecting nodes, O−Z−O (Z = B, C, S, Cr, etc.), and has been applied in the construction of MOFs.[18−20] Such an execution has probably inspired the series of $C(NH_2)_3$ $[Me^{II}(HCOO)_3]$ (Me = Mn,

Received: May 8, 2019
Revised: June 11, 2019
Published: June 20, 2019

Downloaded via NOTTINGHAM TRENT UNIV on August 17, 2019 at 08:49:21 (UTC).
See https://pubs.acs.org/sharingguidelines for options on how to legitimately share published articles.

ACS Publications © 2019 American Chemical Society

DOI: 10.1021/acs.jpcc.9b04368
J. Phys. Chem. C 2019, 123, 18551−18559

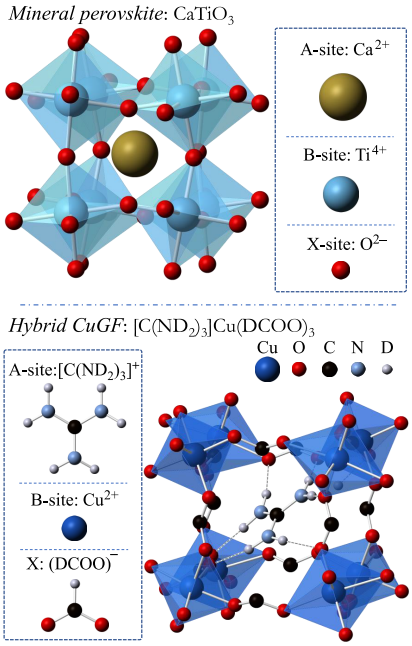

Figure 1. Top: Crystal structure of the mineral *perovskite*: $CaTiO_3$, and the corresponding building units. Bottom: CuO_6 octahedra linked via formates shaping a ReO_3-type cavity housing the guanidinium moiety, replicating the ABX_3 topology; also shown are the individual moieties. For clarity, the *formato*-D atoms are not shown.

Fe, Co, Ni, Cu, and Zn), henceforth referred to as metal guanidinium formates (MeGFs) with an ABX_3 morphology, as presented in Figure 1, enunciating a comparison with the mineral *perovskite*.

With $[C(NH_2)_3]^+$ positioned in the A-site, all the members are orthorhombic with the space group *Pnna*, while copper guanidinium formate (CuGF) is an exception that belongs to the polar space group $Pna2_1$.[21] Me^{2+}, being the octahedral ion interconnecting the neighboring six metal ions via formate ($HCOO^-$) ligands, results in the NaCl-type anionic metal–formate framework with the $4^{12}\cdot6^3$ topology. The $[C(NH_2)_3]^+$ cation is housed in the ReO_3-type cavity and strung to the framework by six hydrogen bonds. The molecular plane of guanidinium is almost normal to the diagonal of the Me–formate cage. Yet, there is a difference in the structure between CuGF and Mn/CoGF, which is attributed to one factor: Jahn–Teller distortion. As Cu^{2+} is a d^9 Jahn–Teller active ion, it gives rise to two elongated apical Cu–O bonds ($d^{Cu-O}_{apical} \approx 2.36–2.38$ Å) with the four other equatorial bonds ($d^{Cu-O}_{equatorial} \approx 1.953–2.003$ Å), resulting in a lower symmetry ($Pna2_1$), allowing six crystallographically nonidentical Cu–O bonds in comparison to Mn/CoGF (*Pnna*) housing three nonidentical Me–O bonds.[21]

All the magnetic members of MeGFs have been identified to exhibit long-range antiferromagnetic ordering.[21] Quite interestingly, from magnetization measurements, CuGF had a broad maximum around 45 K, which could fit with the Bonner–Fisher model,[22] explaining a quasi-1D behavior via strong intrachain coupling through the anti-anti $HCOO^-$ bridge within the formate chain. This low-dimensional magnetic feature had a crossover to 3D antiferromagnetism at lower temperatures.[21] Recent investigations with MeGFs based on neutron scattering have disclosed interesting findings such as the temperature-dependent anomalous mechanics, influence of Jahn–Teller distortion on the enhancement of guest orderliness, disorder in the hydrogen atoms uninvolved in hydrogen bonds, high-pressure phase transitions disregarding group–subgroup association, understanding of the physical mechanism behind the phase transformation as well as structural tunability influenced by uniaxial strength and hydrogen bonding, etc.[23−28]

In an earlier report, *ab initio* calculations have predicted multiferroic characteristics in CuGF based on the polarization attributed to the displacement of the A-site $[C(NH_2)_3]^+$ along the polar-axis.[29] It has been noticed from single-crystal neutron diffraction that there exists no difference between the polar CuGF and its centrosymmetric analogue in terms of the displacement of the guanidinium cation along the polar-axis.[24] Nevertheless, detailed structural investigations provided insights questioning into such predictions.[28] In the same work, the authors have also proposed that CuGF displays a "Type-A" spin arrangement, with two possible solutions, that is, magnetic space groups $Pn'a'2_1$ and $Pna'2_1'$, with the spins directed along the *a* and *c*-axes, respectively. To the best of our knowledge, with no experimental reports on the magnetic structure for any formate-based perovskites, at the time when these experiments were done, it was crucial to shine light on the unknown. Although later, there has been a couple of reports on metal ammonium formates $[NH_4Me^{2+}(HCOO)_3$; Me = Mn, Fe, Co and Ni],[30] cobalt methylammonium formate $[CH_3NH_3][Co(HCOO)_3]$,[31,32] and the *niccolite*-like $[NH_2(CH_3)_2]_n[Fe^{III}M^{II}(HCOO)_6]_n$ and $[(CH_3CH_2)_2NH_2][Fe^{III}Fe^{II}(HCOO)_6]$ compounds.[33−35] In this article, we investigate the magnetic structure of copper guanidinium formate determined by neutron powder diffraction (NPD). By departing ways with the *ab initio* methods, the experimental analysis reveals two possibilities of magnetic structure in CuGF and firmly suggests that the spins lie perpendicular to the polar-axis. In general, this work could provide an encouraging platform for the improvement of *ab initio* methods associated with multiferroic MOFs, which has been acknowledged on its *less mature* stage in comparison to its scenario with inorganic multiferroics.[36] Additionally, we also report the magnetic structure of Mn/CoGF, the centrosymmetric analogues of CuGF by NPD.

EXPERIMENTAL METHODS

Fully deuterated samples of the target materials were prepared by the method described elsewhere,[21] with a slight modification;[23,28] that is, guanidinium chloride was used instead of guanidinium carbonate due to its unavailability in the deuterated form. Powder diffraction measurements were done with the WISH diffractometer[37] at the ISIS Pulsed Neutron and Muon Source, U.K. Rietveld refinements of the nuclear structure were done in the paramagnetic state, and their thermal response is dealt exclusively.[23] The structural and magnetic particulars were initially refined at the highest temperature in the magnetic state, eventually guiding further refinements while climbing down in temperature. Structural-cum-magnetic Rietveld refinements were carried out by using *FullProf*,[38−40] wherein soft restraints were implemented within the guanidinium and formate moiety, as explained in ref 23, leading to meaningful structural attributes. All refinements were performed using the time-of-flight profile function resulting from the convolution of a back-to-back exponential with a Thompson–Cox–Hastings pseudo-Voigt function. In some cases, we have used the option, existing in

DOI: 10.1021/acs.jpcc.9b04368
J. Phys. Chem. C 2019, 123, 18551−18559

FullProf, for working with special reflections, relaxing the local shapes of the profile with respect to the global widths and positions dictated by the cell parameters and resolution function. This improves the profile parameters without affecting the integrated intensities. Backgrounds were modeled using linear interpolation between a set of background points.

MeGFs exhibit spin canting resulting from Dzyaloshinskii–Moriya interactions. The magnitude of spin canting was evaluated from the magnetic hysteresis (canting angle, $\alpha = \sin^{-1} M_R/M_S$) at 2 K.[21] Nevertheless, it is clear from their results that the magnetization at 5 T remains unsaturated for all the MeGFs, and therefore, the actual values of α in principle should have to be smaller than reported, and the same measurements have to be done at sufficiently high magnetic fields to comment on the actual values. In other words, although the reported values of α are inaccurate, in reality, $\alpha^{CoGF} < 4.5°$, $\alpha^{CuGF} < 0.21°$, and $\alpha^{MnGF} < 0.076°$. Such a tiny magnitude of spin canting is below the detection limits of neutron powder diffraction. For this reason, spin canting was not accounted for in the refinements.

RESULTS AND DISCUSSION

Analysis by Representation Theory. The crystallographic space groups of the materials analyzed here are $Pna2_1$ (for CuGF) and *Pnna* (for Mn/CoGF). Further to this, the details of spins such as magnetic moment and direction account for the magnetic structure. Such a representation can be broken down into its irreducible representations (IRs) with the help of group theory.[41] According to Landau's theory of second-order phase transitions, it is one single IR that constitutes the primary order parameter of the phase transition; that is, other basis vectors related to other IRs are necessarily zero, resulting in the advantages of IR.[42] In other words, the number of "symmetry-allowed magnetic structures" is considerably diminished to the number of irreducible magnetic representations.

To determine all magnetic IRs, the propagation vector group (also known as the "little group") $\mathbf{G}_k$ contains all operators of the space group $\mathbf{G}$, leaving the invariant $\mathbf{k}$-vector (point part of the operator converts $\mathbf{k}$ into $\mathbf{k} + \mathbf{H}$, with $\mathbf{H}$ being a reciprocal lattice vector). For the investigated materials, the propagation vector is determined as $\mathbf{k} = (0, 0, 0)$, wherein the magnetic unit cell is identical to the nuclear cell and all operators of $\mathbf{G}$ leave $\mathbf{k}$ invariant, so $\mathbf{G}_k = \mathbf{G} = Pna2_1/Pnna$. While the symmetry analysis may be hand-worked,[43] in this work, BasIreps, a computing program part of the *FullProf suite*,[39] is used. It is noteworthy that magnetic scattering occurs only when the scattering vector $\mathbf{Q}$ is perpendicular to the magnetic field distribution of the sample.[44]

There are four possible magnetic models for $Pna2_1$ and eight in the case of *Pnna*.[45] The complete magnetic representations Γ_{mag} of $\mathbf{G}_k$, broken down into IRs $\Gamma_{k\nu}$ (ν = 1, 2, ...), for CuGF and Mn/CoGF are

$$\Gamma_{mag}^{Pna2_1} = 3\Gamma_{k1} + 3\Gamma_{k2} + 3\Gamma_{k3} + 3\Gamma_{k4} \quad (1)$$

$$\Gamma_{mag}^{Pnna} = 1\Gamma_{k1} + 1\Gamma_{k2} + 2\Gamma_{k3} + 2\Gamma_{k4} + 2\Gamma_{k5} + 2\Gamma_{k6} + 1\Gamma_{k7} + 1\Gamma_{k8} \quad (2)$$

All the basis vectors Ψ_n and the Shubnikov group (Sh.G.) corresponding to each IR are listed in the Supporting Information. The magnetic moment of an atom is obtained as a linear combination of the basis vectors corresponding to a specific IR, $m_j = \sum_n C_n \Psi_n$.

Magnetic Structure of the "Polar" Copper Guanidinium Formate. The four IRs of the $Pna2_1$ space group correspond to the following magnetic groups in Shubnikov notation and *modes* are Γ_{k1} :: $Pna2_1$ (G_x A_y C_z), Γ_{k2} :: $Pn'a'2_1$ (A_x G_y F_z), Γ_{k3} :: $Pn'a2_1'$ (C_x F_y G_z), and Γ_{k4} :: $Pna'2_1'$ (F_x C_y A_z). While, in the theoretical work by Stroppa et al.,[29] it was proposed that CuGF displays "Type-A" spin arrangement, that is, ferromagnetic ordering within the plane (*intraplanar*-FM) and antiferromagnetic ordering between adjacent planes (*interplanar*-AFM), and is permissible by two magnetic space groups, $Pn'a'2_1$ (Γ_{k2}) and $Pna'2_1'$ (Γ_{k4}), with the spins directed along the *a* and *c*-axes, respectively, we notice the monochrome magnetic space group $Pna2_1$ where a Type-A arrangement with moments along the *b*-axis is also possible. The experimentally measured diffraction pattern at 1.5 K is shown in Figure 2a. The "*pristine* magnetic signature" (nuclear-free) obtained from the difference in the intensity of the magnetic state (at 1.5 K) and paramagnetic state (5 K), as shown in Figure 2b, manifests the exclusive presence of the weak (001) magnetic peak at 11.267 Å and the absence of any other magnetic signature. The magnetic peak (001) presents information on the *a* and *b* components, as neutrons are sensitive to the magnetic moments perpendicular to the scattering vector. With the absence of magnetic intensity in the (100) peak at 8.415 Å and the (010) peak at 9.023 Å, these observations suggest that the moments are perpendicular to the *c*-axis. Rietveld refinements were done for all the four IRs (Γ_{k1}–Γ_{k4}).

The analysis suggests that Γ_{k3} and Γ_{k4} are not the solutions due to the absence of magnetic intensity associated with (001), and therefore are ruled out. The solutions Γ_{k1} and Γ_{k2} are too close to be distinguished with the present set of data. Figure 2c displays the comparative simulated magnetic pattern for all IRs, wherein the peaks at $d \approx 3.95$ and 4.2 Å (indicated by the reference markers) are the distinguishable factors. Due to their inherent low-intense nature, it becomes unfeasible to differentiate between Γ_{k1} and Γ_{k2}. Although the magnetic R-factor (bank 1) of Γ_{k1} (5.03%) is better than Γ_{k2} (15.2%), it is notable that the refinement statistics are at their very limits due to the weak magnetic signature.

$Pna2_1$ (Γ_{k1}) is a purely antiferromagnetic scenario, which also is the model giving the better fit to the neutron data. The results based on this magnetic solution suggests that the A-*mode* is dominant. This solution reveals a "Type-A" spin arrangement. Here, the spins are directed along the *b*-axis (see Figure 2d) with $|\boldsymbol{m}| \approx 0.63(10)$ μ_B whose antiferromagnetic interactions are along the *c*-axis. Unlike Γ_{k1}, in Γ_{k2}, a ferromagnetic component is allowed. The absence of any additional magnetic intensity on the top of the nuclear Bragg peak reveals the absence of any F-*mode*. A simulated pattern considering the F-*mode* of Γ_{k2} is shown in Figure 3. Further, as macroscopic magnetic measurements exhibit no saturation even at a sufficiently high magnetic field (H_{max} = 5 T),[21] suggesting strong antiferromagnetic interactions, in the refinements, the F-*mode* was fixed to 0.

While the evaluation of the magnetic structure from neutron diffraction suggesting the "Type-A" spin arrangement in CuGF is supportive of the *ab initio* studies, the exact magnetic structure solution is accompanied by a difference. Although *ab initio* calculations[29] are suggestive of the

DOI: 10.1021/acs.jpcc.9b04368
J. Phys. Chem. C 2019, 123, 18551–18559

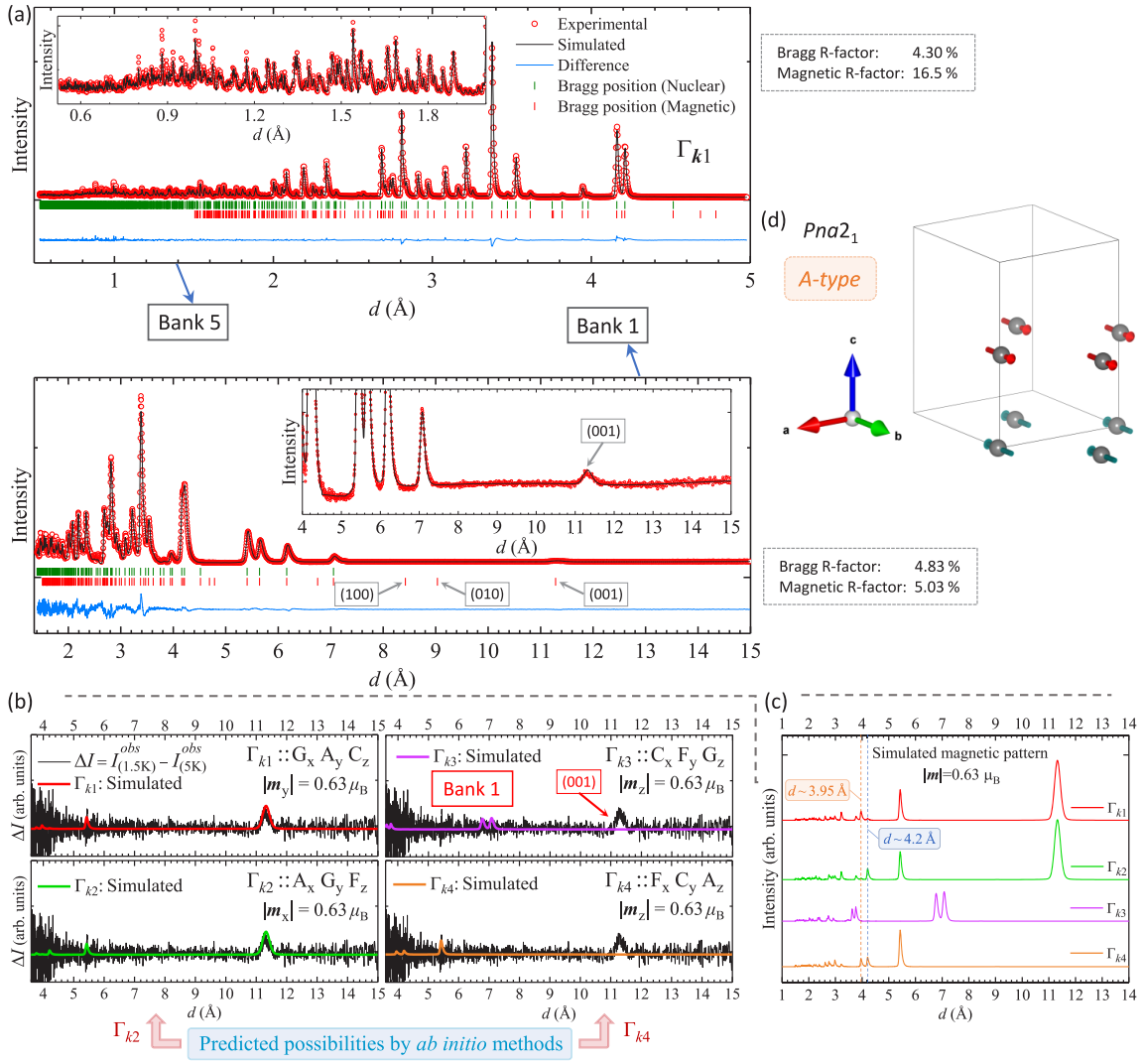

Figure 2. (a) Magnetic refinement of the powder diffraction pattern of CuGF at 1.5 K for the Shubnikov group $Pna2_1$ (Γ_{k1}) suggests the "Type-A" spin arrangement. Top: Powder pattern collected with the high-angle detector (bank 5). Bottom: Powder pattern collected from the low-angle detector (bank 1). (b) Pristine magnetic signature obtained from the difference between 1.5 and 5 K presenting the (001) magnetic peak and the overlay of the corresponding simulated magnetic solutions for $|m| = 0.63\ \mu_B$. (c) Comparative simulated patterns for Γ_{k1}–Γ_{k4}. (d) "Type-A" spin arrangement in CuGF presented with the counter-spins exclusively along the *c*-axis. The magnetic structure images shown in this work are generated using the VESTA program.[49]

magnetic space group as $Pn'a'2_1$ (Γ_{k2}) or $Pna'2_1'$ (Γ_{k4}), experimentally, the magnetic space group of CuGF can be assigned to either $Pna2_1$ (Γ_{k1}) or $Pn'a'2_1$ (Γ_{k2}), with spins directed along the *b* or *a*-axes, respectively, concurrently ruling out the possibility of the spins being directed along the polar-axis. With such a difference in comparison with the *ab initio* studies, we are reminded that the current investigations based on neutron powder diffraction are at the very limits of the experimental technique itself. Perhaps, much more sophisticated tools such as single-crystal neutron diffraction might be useful to resolve the magnetic peaks at the *d*-window of 3.5–4.5 Å, henceforth arriving at the exact magnetic structure.

Evaluation of Spin States in the Centrosymmetric Mn/Co Guanidinium Formate. The theoretically possible spin configurations of the investigated divalent metals in octahedral coordination are shown in Figure 4 (top panel). The inset table lists the corresponding spin-only moment for S = $^1/_2$, $^3/_2$, and $^5/_2$. Cu^{2+}, being a d^9 system, can present

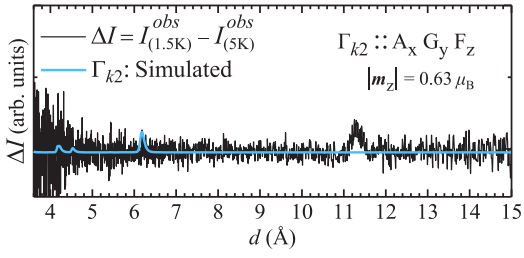

Figure 3. Simulated magnetic solution for Γ_{k2} exclusively to the F-*mode* in comparison to the pristine magnetic signature, suggesting the absence of the F-*mode*.

with just one spin state, S = $^1/_2$. Contrastingly, Mn^{2+} and Co^{2+} can have multiple configurations. To determine the exact spin state, the effective paramagnetic moment is calculated from χ^{-1} obtained from magnetization measured at a constant applied field of 10 Oe using a SQUID magnetometer, and is shown in Figure 4 (bottom panel). The

DOI: 10.1021/acs.jpcc.9b04368
J. Phys. Chem. C 2019, 123, 18551−18559

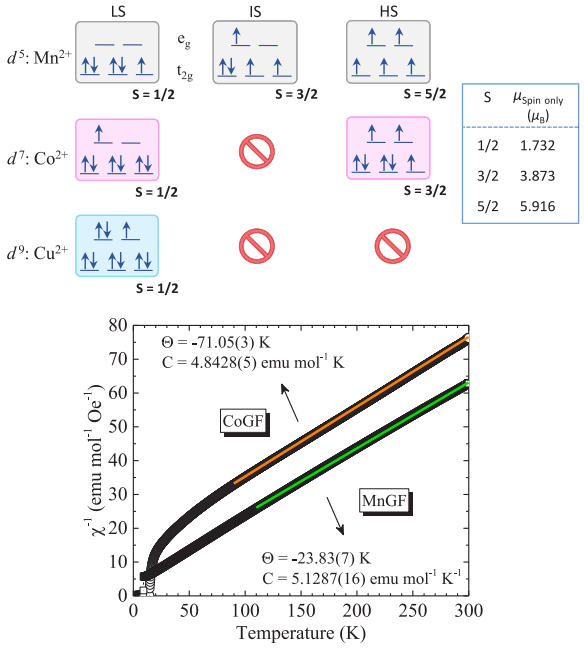

Figure 4. Top: Possible spin states for the d^5 (Mn^{2+}), d^7 (Co^{2+}), and d^9 (Cu^{2+}) ions and their corresponding spin-only moments, μ_{so} = $[4S(S+1)]^{1/2}$. Bottom: Inverse susceptibility and corresponding Curie–Weiss fit for protonated MnGF and CoGF under an applied magnetic field, H_{DC} = 10 Oe.

negative intercept, representing the Weiss temperature (Θ), reaffirms the long-range antiferromagnetic ordering reported earlier for both MnGF and CoGF.[21] The determined Curie constant and the effective moment (μ_{eff}) for MnGF are 5.129 emu mol^{-1} K^{-1} and 6.4 μ_B, respectively. Likewise, the corresponding values for CoGF are 4.843 emu mol^{-1} K^{-1} and 6.22 μ_B.

While the μ_{eff} of MnGF is slightly higher than anticipated, the value for CoGF is much higher than the predicted one (μ_{so} = 3.873 μ_B). This discrepancy exists, as transition metal ions although exhibit diminutive values of L, Co^{2+} was found to exhibit a prominent unquenched L in CoO.[46] It is this feature that establishes versatility on the magnetism of Co^{2+} systems, also being influenced by the Co–O bond length impacting the crystal field and, hence, its properties.[47,48] Therefore, the higher value of μ_{eff} is due to the spin-only assumption, which excludes L. Regardless, the μ_{eff} of both MnGF and CoGF can unambiguously be attributed to their high-spin states, that is, Mn^{2+} (HS: t_{2g}^3, e_g^2) and Co^{2+} (HS: t_{2g}^5, e_g^2), respectively. These results are important and in agreement with magnetic diffraction. In general, such an influence of magnetometry, adding an assertion, is underappreciated and, when exploited, could yield into a right combination with neutron diffraction, helping one to assess the right magnetic structural model.

Magnetic Structure of Mn/Co Guanidinium Formate. Both MnGF and CoGF exhibit a difference in the intensities between the paramagnetic state and magnetically ordered

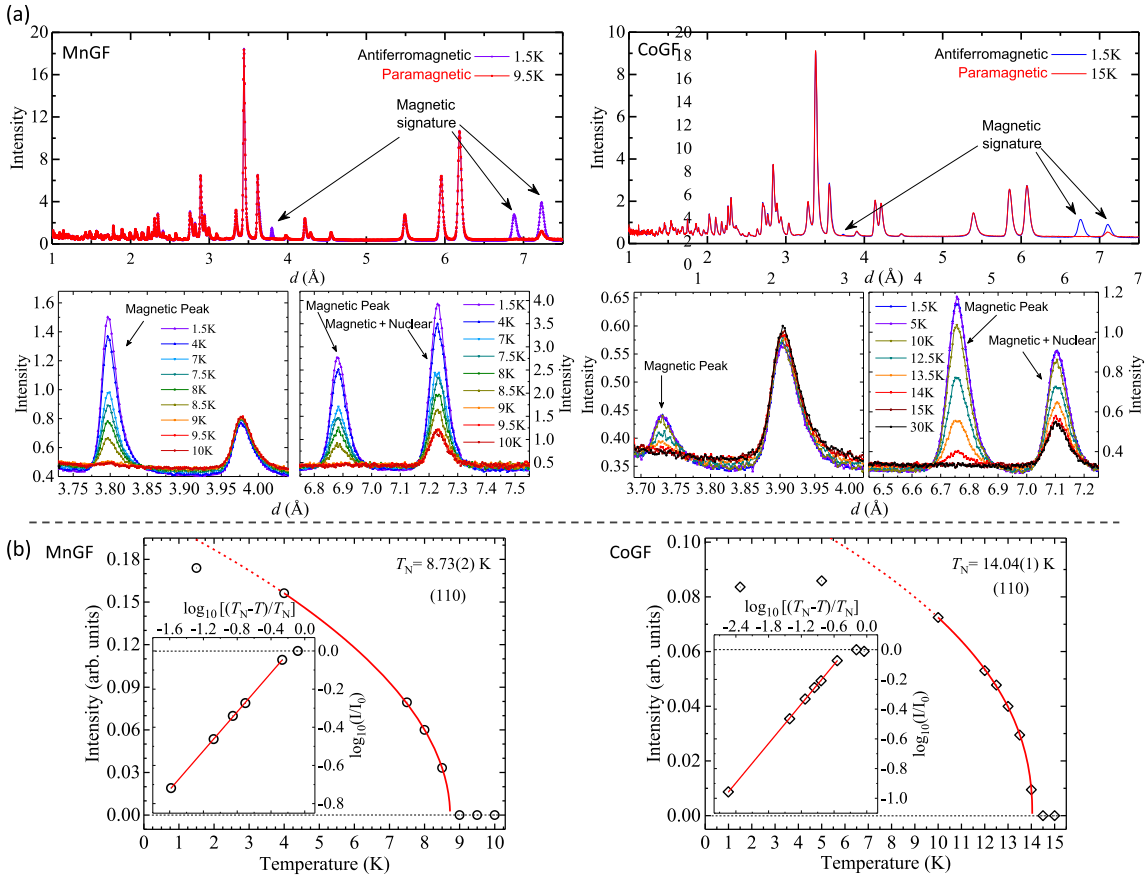

Figure 5. (a) Top: Comparative diffraction patterns in paramagnetic and ordered states show the visible signature of the magnetic intensity. Bottom: Representation of magnetic intensities at different temperatures across a chosen window for Mn/CoGF. (b) Temperature dependence of $I(110)$ for Mn/CoGF and its fit to power-law $I(T)$ = $[1 - (T/T_N)]^{2\beta}$. Insets show the log–log plot of the same data.

DOI: 10.1021/acs.jpcc.9b04368
J. Phys. Chem. C 2019, 123, 18551–18559

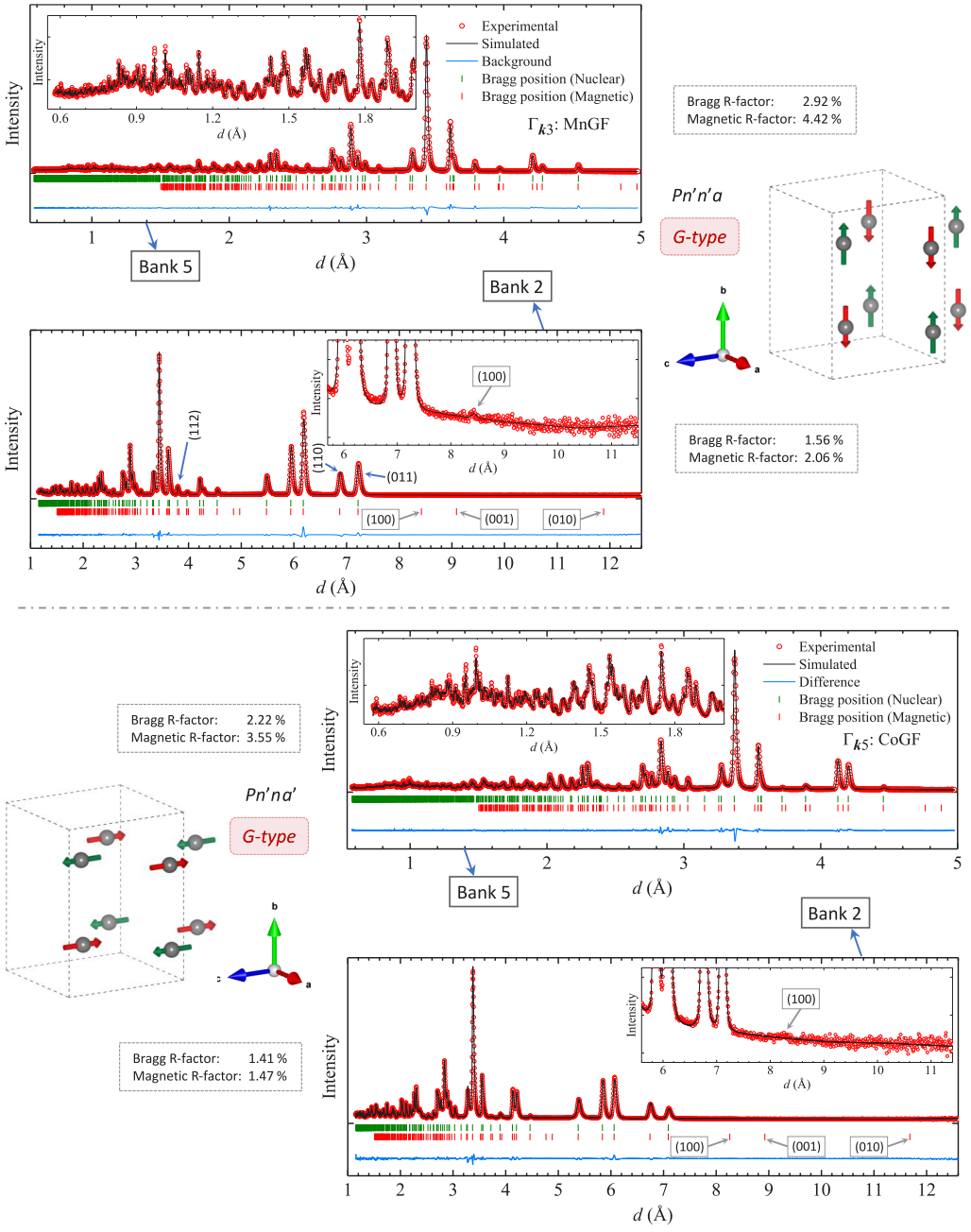

Figure 6. Top: Magnetic refinements of the powder diffraction pattern (at 1.5 K) of MnGF (Γ_{k3}) and CoGF (Γ_{k5}). Bottom: Outcome of the magnetic refinements as shown by the spin arrangements, whereby both the models suggest a "G-type" antiferromagnetic ordering yet differ on their direction of moments.

state. Figure 5a shows the neutron diffraction pattern of MnGF at 1.5 K in the magnetic state and at 9.5 K in the paramagnetic state, collected from bank 3. For MnGF, an exclusive magnetic peak at around 6.8 Å (110) exists along with two other peaks growing on the top of the nuclear signature at around 3.8 Å (112) and 7.25 Å (011), with similar features in the isostructural CoGF. The temperature dependence of these peaks is represented in the bottom panel. The (112) magnetonuclear peak of MnGF has more electronic contribution in comparison to CoGF; that is, at low temperatures, its growth in intensity for MnGF is higher than that for CoGF. Neutrons being sensitive to magnetic moments perpendicular to **Q**, the (110) peak has information on the *c* component of the moment, while the (011) contains the *a* component. In terms of the ratio of the intensity, it is notable that $I^{\mathrm{MnGF}}_{(110)/(011)} < I^{\mathrm{CoGF}}_{(110)/(011)}$. The magnetic information to be extracted depends on the information dependent on these peaks to a larger extent.

The temperature dependence of the intensities of the magnetic peaks has a simple power-law relationship[50] as the integrated intensity of the magnetic peak is proportional to the square of the ordered moment. The integrated intensity of the "strong" magnetic reflection (011) is made to account for its temperature dependence. Although the lack of a higher number of data points near T_N restricts in obtaining the critical exponent, the data sets convincingly provide a decent value of T_N. Figure 5b displays the same for the target

DOI: 10.1021/acs.jpcc.9b04368
J. Phys. Chem. C 2019, 123, 18551−18559

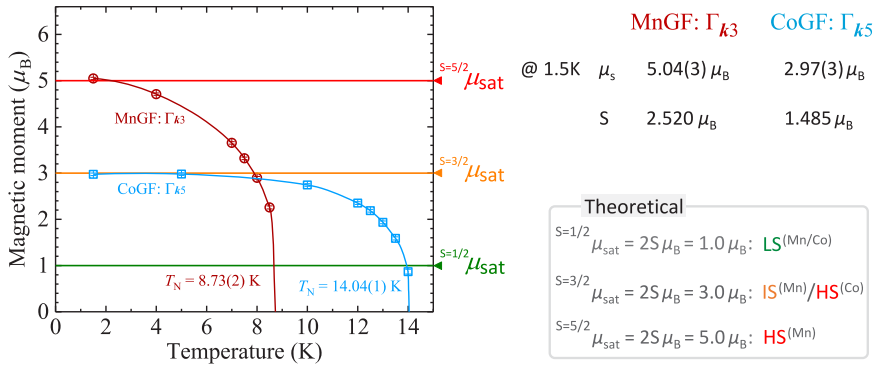

Figure 7. Left: Magnetic moment obtained from the refined models Γ_{k3} and Γ_{k5}; the solid lines are a guide to the eye. Right: Corresponding values of magnetic moment at 1.5 K and associated spin values highlighting its closeness with the Co^{2+} high-spin state. Theoretical values obtained from the relation $\mu_{Sat} = gJ\mu_B \Rightarrow \mu_{Sat} = 2S\mu_B$ for the $J = S$ scenario.[51,52]

materials and reveals that T_N^{MnGF} = 8.73(2) K and T_N^{CoGF} = 14.04(1) K.

Magnetic Rietveld refinements were attempted for all the IRs (Γ_{k1}–Γ_{k8}), which converges to two possibilities of Γ_{k3} and Γ_{k5}, both suggesting an antiferromagnetic ordering. All the magnetic peaks are fulfilled by the magnetic refinement of Γ_{k3}(MnGF) and Γ_{k5}(CoGF). Representative Rietveld fits for data collected at 1.5 K are shown in Figure 6 for both MnGF and CoGF. Two of the detector banks were accounted for, in the refinement. Both the models suggest an antiferromagnetic ordering, with each spin having counter-spins as its neighbors, which is the distinctive signature of "Type-G" magnetic ordering. However, it is the direction in which the spins are oriented that differs among them. A closer inspection shows that Mn/CoGF account for the absence of magnetic intensity in (010) and (001) peaks yet present with a weak (100) peak, as shown in the inset of the respective diffraction profile (bank 2) in Figure 6. This feature is suggestive of the magnetic moments perpendicular to the *a*-axis.

When magnetic fits are attempted with the alternative solution, that is, Γ_{k5}(MnGF) and Γ_{k3}(CoGF), at least one of the magnetic peaks does not fit the experimental data well enough. With such a justification, the magnetic structures of MnGF based on "Γ_{k3}" and CoGF based on "Γ_{k5}" are concluded as *Pn′n′a* and *Pn′na′*, respectively. This is a notable difference between the magnetic structures of MnGF and CoGF, exhibiting spin alignment along the *b* and *c* axes, respectively.

The evaluated magnetic moments of Mn^{2+} and Co^{2+} from the refinement at temperatures below T_N are shown in Figure 7. Both of them indicate high values of saturation magnetic moment with μ_{Sat}(MnGF) > μ_{Sat}(CoGF). These values reflect the high-spin states; that is, (i) for Mn^{2+}, it is HS (t_{2g}^3, e_g^2) and is quite far from two of its alternatives, LS (t_{2g}^5, e_g^0) and IS (t_{2g}^4, e_g^1); (ii) for Co^{2+}, it is HS (t_{2g}^5, e_g^2) and is quite far off to the alternative Co^{2+} (LS: t_{2g}^6, e_g^1). These results are endorsed by the Curie–Weiss fit obtained from magnetometry, adding credibility to the assessment by magnetic neutron diffraction. The values of the magnetic moment obtained from the refinement are convincing (shown by the reference marker in Figure 7) and supportive to the perspective on the spin states obtained by magnetometry.

CONCLUSIONS

In summary, from our experimental studies based on neutron powder diffraction, the magnetic structure of the hybrid perovskite "copper guanidinium formate" is found to exhibit "Type-A" antiferromagnetic ordering. Our investigations rule out *Pna′2₁′* (Γ_{k4}), one of the two originally assigned possibilities by *ab initio* calculations. Unlike earlier studies, we show that the monochrome magnetic space group $Pna2_1$ (Γ_{k1}) is also permissible to exhibit "Type-A" magnetic ordering. Being at the limits of experimental probing via neutron powder diffraction, herein, the magnetic structure solution could be reassigned to either $Pna2_1$ (Γ_{k1}) or $Pn'a'2_1$ (Γ_{k2}), concurrently eliminating the possibility of the spins along the polar-axis. With determination of the magnetic structure in hybrid materials being in its infancy and, with growing interests in multiferroic MOFs, our experimental results provide a clearer picture on CuGF, a promised multiferroic that lacks "ferromagnetic interactions" along the "polar-axis". In addition, Mn/CoGF, the centrosymmetric analogues by contrast, exhibit "Type-G" magnetic ordering, with a notable difference in the direction of the spin alignment. Evaluation of spin states from magnetization measurements reveal the high-spin nature of the ions in the studied compounds, which is in very good agreement with the results of magnetic diffraction. This rare study probing the magnetic structure of a family of MOFs uncovers information on the spins contrasting to the predictions based on *ab initio* calculations. Therefore, this study helps with the designing of magnetic functionalities in multiferroic hybrid materials by dispensing additional magnetically lucid information for future *ab initio* studies.

ASSOCIATED CONTENT

Supporting Information

The Supporting Information is available free of charge on the ACS Publications website at DOI: 10.1021/acs.jpcc.9b04368.

Basis vectors associated with relevant irreducible representations for the target materials (PDF)

AUTHOR INFORMATION

Corresponding Author

*E-mail: viswanathan.mohandoss@outlook.com; viswanathan@qmul.ac.uk.

ORCID

M. Viswanathan: 0000-0002-2187-2583

Notes

The authors declare no competing financial interest.

DOI: 10.1021/acs.jpcc.9b04368
J. Phys. Chem. C 2019, 123, 18551–18559

■ ACKNOWLEDGMENTS

The authors are thankful to STFC for providing neutron beamtime at ISIS Pulsed Neutron and Muon Source, as well as Dr. D. D. Khalyavin, Dr. P. Manuel, and Dr. M. J. Gutmann for the help with data collection and a critical read-through of the manuscript. M.V. and S.G.B. thank Professor P. S. Anil Kumar for valuable discussions. M.V. is thankful to Professor William Gillin and Professor Mike Watkinson for the discussions on the manuscript and their overall advice on academic matters and also acknowledges QMUL for the funding through the College Doctoral Training Award.

■ REFERENCES

(1) Eerenstein, W.; Mathur, N. D.; Scott, J. F. Multiferroic and magnetoelectric materials. *Nature* **2006**, *442*, 759−765.
(2) Yaghi, O. M.; O'Keeffe, M.; Ockwig, N. W.; Chae, H. K.; Eddaoudi, M.; Kim, J. Reticular synthesis and the design of new materials. *Nature* **2003**, *423*, 705−714.
(3) Cheetham, A. K.; Rao, C. N. R. There's room in the middle. *Science* **2007**, *318*, 58−59.
(4) Wang, X.-Y.; Wang, Z.-M.; Gao, S. A pillared layer MOF with anion-tunable magnetic properties and photochemical [2 + 2] cycloaddition. *Chem. Commun.* **2007**, 1127−1129.
(5) Wollan, E. O.; Koehler, W. C. Neutron diffraction Study of the magnetic properties of the series of perovskite-type compounds [(1-*x*)La, *x*Ca] MnO_3. *Phys. Rev.* **1955**, *100*, 545.
(6) Takeda, T.; Õhara, S. Magnetic structure of the cubic perovskite type $SrMnO_3$. *J. Phys. Soc. Jpn.* **1974**, *37*, 275.
(7) Quezel, S.; Tcheou, F.; Rossat-Mignod, J.; Quezel, G.; Roudaut, E. Magnetic structure of the perovskite-like compound $TbMnO_3$. *Physica B+C* **1977**, *86-88*, 916−918.
(8) Muñoz, A.; Alonso, J. A.; Casais, M. T.; Martínez-Lope, M. J.; Martínez, J. L.; Fernández-Díaz, M. T. The magnetic structure of $YMnO_3$ perovskite revisited. *J. Phys.: Condens. Matter* **2002**, *14*, 3285−3294.
(9) Moritomo, Y.; Xu, S.; Machida, A.; Akimoto, T.; Nishibori, E.; Takata, M.; Sakata, M.; Ohoyama, K. Crystal and magnetic structure of conducting double perovskite Sr_2FeMoO_6. *J. Phys. Soc. Jpn.* **2000**, *69*, 1723−1726.
(10) Muñoz, A.; Alonso, J. A.; Casais, M. T.; Martínez-Lope, M. J.; Fernández-Díaz, M. T. Crystal and magnetic structure of the complex oxides Sr_2MnMoO_6, Sr_2MnWO_6 and Ca_2MnWO_6: a neutron diffraction study. *J. Phys.: Condens. Matter* **2002**, *14*, 8817−8830.
(11) Hosaka, Y.; Ichikawa, N.; Saito, T.; Manuel, P.; Khalyavin, D.; Paul Attfield, J.; Shimakawa, Y. Two-dimensional charge disproportionation of the unusual high valence state Fe^{4+} in a layered double perovskite. *J. Am. Chem. Soc.* **2015**, *137*, 7468−7473.
(12) Blake, G. R.; Chapon, L. C.; Radaelli, P. G.; Park, S.; Hur, N.; Cheong, S.-W.; Rodríguez-Carvajal, J. Spin structure and magnetic frustration in multiferroic RMn_2O_5 (R=Tb,Ho,Dy). *Phys. Rev. B* **2005**, *71*, 214402.
(13) Christianson, A. D.; Lumsden, M. D.; Angst, M.; Yamani, Z.; Tian, W.; Jin, R.; Payzant, E. A.; Nagler, S. E.; Sales, B. C.; Mandrus, D. Three-dimensional magnetic correlations in multiferroic $LuFe_2O_4$. *Phys. Rev. Lett.* **2008**, *100*, 107601.
(14) Figueiras, F. G.; Karpinsky, D.; Tavares, P. B.; Das, S.; Leitão, J. V.; Brück, E. H.; Agostinho Moreira, J. ; Amaral, V. S. Breaking the geometric magnetic frustration in controlled off-stoichiometric $LuMn_{1+z}O_{3+\delta}$ compounds. *Phys. Chem. Chem. Phys.* **2016**, *18*, 13519−13523.
(15) Figueiras, F. G.; Karpinsky, D.; Tavares, P. B.; Gonçalves, J. N.; Yañez-Vilar, S.; Moreira Dos Santos, A. F.; Franz, A.; Tovar, M.; Agostinho Moreira, J.; Amaral, V. S. Novel multiferroic state and ME enhancement by breaking the AFM frustration in $LuMn_{1-x}O_3$. *Phys. Chem. Chem. Phys.* **2017**, *19*, 1335−1341.
(16) Suresh, P.; Vijaya Laxmi, K.; Bera, A. K.; Yusuf, S. M.; Chittari, B. L.; Jung, J.; Anil Kumar, P. S. Magnetic ground state of the multiferroic hexagonal $LuFeO_3$. *Phys. Rev. B* **2018**, *97*, 184419.
(17) Jain, P.; Ramachandran, V.; Clark, R. J.; Zhou, H. D.; Toby, B. H.; Dalal, N. S.; Kroto, H. W.; Cheetham, A. K. Multiferroic behavior associated with an order−disorder hydrogen bonding transition in metal−organic frameworks (MOFs) with the perovskite ABX_3 architecture. *J. Am. Chem. Soc.* **2009**, *131*, 13625−13627.
(18) Abrahams, B. F.; Haywood, M. G.; Hudson, T. A.; Robson, R. Cubic, Hydrogen-bonded (10,3)-*a* networks in the family $[C(NH_2)_3][N(CH_3)_4][XO_4]$ (X=S, Cr, and Mo). *Angew. Chem., Int. Ed.* **2004**, *43*, 6157−6160.
(19) Abrahams, B. F.; Hawley, A.; Haywood, M. G.; Hudson, T. A.; Robson, R.; Slizys, D. A. Serendipity and design in the generation of new coordination polymers: an extensive series of highly symmetrical guanidinium-templated, carbonate-based networks with the sodalite topology. *J. Am. Chem. Soc.* **2004**, *126*, 2894−2904.
(20) Abrahams, B. F.; Haywood, M. G.; Robson, R. Guanidinium ion as a symmetrical template in the formation of cubic hydrogen-bonded borate networks with the boracite topology. *J. Am. Chem. Soc.* **2005**, *127*, 816−817.
(21) Hu, K.-L.; Kurmoo, M.; Wang, Z.; Gao, S. Metal-Organic Perovskites: Synthesis, structures, and magnetic properties of $[C(NH_2)_3][M^{II}(HCOO)_3]$ (M=Mn, Fe, Co, Ni, Cu, and Zn; $C(NH_2)_3$= guanidinium). *Chem. − Eur. J.* **2009**, *15*, 12050−12064.
(22) Bonner, J. C.; Fisher, M. E. Linear magnetic chains with anisotropic coupling. *Phys. Rev.* **1964**, *135*, A640.
(23) Viswanathan, M. Neutron diffraction studies on the thermal expansion and anomalous mechanics in the perovskite-type $[C(ND_2)_3]Me^{2+}(DCOO)_3$ [Me = Cu, Mn, Co]. *Phys. Chem. Chem. Phys.* **2018**, *20*, 17059−17070.
(24) Viswanathan, M. Enhancement of the guest orderliness in a low-symmetric perovskite-type metal−organic framework influenced by Jahn−Teller distortion. *Phys. Chem. Chem. Phys.* **2018**, *20*, 21809−21813.
(25) Viswanathan, M. Disorder in the hydrogen-atoms uninvolved in hydrogen bonds in a metal−organic framework. *Phys. Chem. Chem. Phys.* **2018**, *20*, 24527−24534.
(26) Viswanathan, M. High-pressure phase transitions with group−subgroup disagreement in metal guanidinium formates. *CrystEngComm* **2018**, *20*, 6861−6866.
(27) Viswanathan, M. Structural tunability Controlled by uniaxial strength in a hybrid perovskite. *J. Phys. Chem. C* **2019**, *123*, 6711−6716.
(28) Mohandoss, Viswanathan. *Structure, Magnetic Ground States and Phase Transitions in Metal Guanidinium Formates*; PhD dissertation, Queen Mary University of London (UK), 2017.
(29) Stroppa, A.; Jain, P.; Barone, P.; Marsman, M.; Perez-Mato, J. M.; Cheetham, A. K.; Kroto, H. W.; Picozzi, S. Electric control of magnetization and interplay between orbital ordering and ferroelectricity in a multiferroic metal-organic framework. *Angew. Chem., Int. Ed.* **2011**, *50*, 5847−5850.
(30) Lawler, J. M. M.; Manuel, P.; Thompson, A. L.; Saines, P. J. Probing ferroic transitions in a multiferroic framework family: a neutron diffraction study of the ammonium transition metal formates. *Dalton Trans.* **2015**, *44*, 11613−11620.
(31) Gómez-Aguirre, L. C.; Pato-Doldán, B.; Mira, J.; Castro-García, S.; Señarís-Rodríguez, M. A.; Sánchez-Andújar, M.; Singleton, J.; Zapf, V. S. Magnetic ordering-induced multiferroic behavior in $[CH_3NH_3][Co(HCOO)_3]$ metal−organic framework. *J. Am. Chem. Soc.* **2016**, *138*, 1122−1125.
(32) Mazzuca, L.; Cañadillas-Delgado, L.; Fabelo, O.; Alberto Rodríguez-Velamazán, J.; Luzón, J.; Vallcorba, O.; Simonet, V.; Colin, C. V.; Rodríguez-Carvajal, J. Microscopic insights on the multiferroic perovskite-like $[CH_3NH_3][Co(COOH)_3]$ compound. *Chem. − Eur. J.* **2018**, *24*, 388−399.
(33) Cañadillas-Delgado, L.; Fabelo, O.; Alberto Rodríguez-Velamazán, J.; Lemée-Cailleau, M.-H.; Mason, S. A.; Pardo, E.;

DOI: 10.1021/acs.jpcc.9b04368
J. Phys. Chem. C 2019, 123, 18551−18559

Lloret, F.; Zhao, J.-P.; Bu, X.-H.; Simonet, V.; Colin, C. V.; Rodríguez-Carvajal, J. The role of order−disorder transitions in the quest for molecular multiferroics: structural and magnetic neutron studies of a mixed valence iron(II)−iron(III) formate framework. *J. Am. Chem. Soc.* **2012**, *134*, 19772−19781.
(34) Mazzuca, L.; Cañadillas-Delgado, L.; Alberto Rodríguez-Velamazán, J.; Fabelo, O.; Scarrozza, M.; Stroppa, A.; Picozzi, S.; Zhao, J.-P.; Bu, X.-H.; Rodríguez-Carvajal, J. Magnetic structures of heterometallic M(II)−M(III) formate compounds. *Inorg. Chem.* **2017**, *56*, 197−207.
(35) Zhao, J.-P.; Xu, J.; Han, S.-D.; Wang, Q.-L.; Bu, X.-H. A Niccolite Structural Multiferroic Metal-organic framework possessing four different types of bistability in response to dielectric and magnetic modulation. *Adv. Mater.* **2017**, *29*, 1606966.
(36) Stroppa, A. Polar and magneto-electric properties of antiferrodistortive ordered Jahn-Teller distortions in a multiferroic metal-organic framework. *J. Phys.: Conf. Ser.* **2013**, *428*, No. 012029.
(37) Chapon, L. C.; Manuel, P.; Radaelli, P. G.; Benson, C.; Perrott, L.; Ansell, S.; Rhodes, N. J.; Raspino, D.; Duxbury, D.; Spill, E.; Norris, J. Wish: The new powder and single crystal magnetic diffractometer on the second target station. *Neutron News* **2011**, *22*, 22−25.
(38) Rodriguez-Carvajal, J. FullProf: A Program for Rietveld Refinement and Pattern Matching Analysis. In *Satellite meeting on powder diffraction of the XV congress of the IUCr*; International Union of Crystallography: Toulouse, France, 1990, 127.
(39) Rodríguez-Carvajal, J. Recent advances in magnetic structure determination by neutron powder diffraction. *Physica B* **1993**, *192*, 55−69.
(40) The programs, news, and documentation concerning the *FullProf Suite* can be found in the website https://www.ill.eu/sites/fullprof.
(41) Bertaut, E. F. Representation analysis of magnetic structures. *Acta Crystallogr., Sect. A: Cryst. Phys., Diffr., Theor. Gen. Crystallogr.* **1968**, *24*, 217−231.
(42) Authier, A., Ed. *International Tables for Crystallography, Volume D: Physical properties of crystals*; Kluwer Academic Publishers Netherlands: 2003.
(43) Schweizer, J. Structures magnétiques et symétries cristallines. *J. Phys. IV* **2001**, *11*, Pr9-105−Pr9-132.
(44) The magnetic moment of a neutron is $\mu_n = -\gamma\mu_N\sigma$, where γ, μ_N, and σ are the gyromagnetic ratio, nuclear magneton, and magnetic dipole moment, respectively. Magnetic scattering arises due to the interactions between μ_n and **B**, the magnetic field within the sample, originating from the spin and orbital momentum of unpaired electrons. The interaction potential in spatial coordinates is $V_M(\mathbf{r}) = -\mu_n \cdot \mathbf{B}(\mathbf{r})$. The Fourier transform of the interaction potential, which is necessary in determining the cross section, relates the local magnetic field and local magnetization and is represented as $V_M(\mathbf{Q}) = -\mu_n \cdot \mathbf{B}(\mathbf{Q}) = -\gamma\mu_N\sigma\mu_0 \cdot \mathbf{M}_\perp(\mathbf{Q})$, which effectively is the condition for magnetic scattering to occur.
(45) Stokes, H. T.; Campbell, B. J. *Table of Magnetic Space Groups*. http://stokes.byu.edu/iso/magneticspacegroups.php. Access reaffirmed on 11 June 2019.
(46) Ghiringhelli, G.; Tjeng, L. H.; Tanaka, A.; Tjernberg, O.; Mizokawa, T.; de Boer, J. L.; Brookes, N. B. 3*d* spin-orbit photoemission spectrum of nonferromagnetic materials: The test cases of CoO and Cu. *Phys. Rev. B* **2002**, *66*, No. 075101.
(47) Csiszar, S. I.; Haverkort, M. W.; Hu, Z.; Tanaka, A.; Hsieh, H. H.; Lin, H.-J.; Chen, C. T.; Hibma, T.; Tjeng, L. H. Controlling orbital moment and spin orientation in CoO layers by strain. *Phys. Rev. Lett.* **2005**, *95*, 187205.
(48) Viswanathan, M.; Hsieh, H. H.; Lin, H.-J.; Chen, C. T.; Anil Kumar, P. S. Investigation on the magnetic anomaly and the role of orbital moment on the magnetic properties of $LaMn_{0.5}Co_{0.5}O_3$. *J. Phys. Chem. C* **2011**, *115*, 4851−4855.
(49) Momma, K.; Izumi, F. *VESTA* 3 for three-dimensional visualization of crystal, volumetric and morphology data. *J. Appl. Crystallogr.* **2011**, *44*, 1272−1276.
(50) Collins, M. F. *Magnetic Critical Scattering*; Oxford Series on Neutron Scattering in Condensed Matter; Oxford University Press: New York, U.S.A., 1989.
(51) Chikazumi, S. *Physics of Ferromagnetism (The International Series of Monographs on Physics)*; The International Series of Monographs on Physics; Oxford University Press: Oxford, U.K., 2 ed., 2009.
(52) Blundell, S. *Magnetism in Condensed Matter*; Oxford Master Series in Condensed Matter Physics; Oxford University Press: Oxford, U.K., 2001.

DOI: 10.1021/acs.jpcc.9b04368
J. Phys. Chem. C 2019, 123, 18551−18559